AD-A228 943

TEM Lattice Imaging of the Nanostructure of Early-Growth Sputter-Deposited MoS₂ Solid Lubricant Films

M. R. HILTON and P. D. FLEISCHAUER
Chemistry and Physics Laboratory
Laboratory Operations
The Aerospace Corporation
El Segundo, CA 90245-4691

DTIC
ELECTE
NOV 15 1990
D

30 September 1990

Prepared for

SPACE SYSTEMS DIVISION
AIR FORCE SYSTEMS COMMAND
Los Angeles Air Force Base
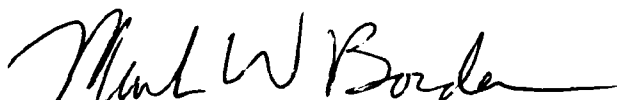P.O. Box 92960
Los Angeles, CA 90009-2960

90

This report was submitted by The Aerospace Corporation, El Segundo, CA 90245, under Contract No. F04701-88-C-0089 with the Space Systems Division, P.O. Box 92960, Los Angeles, CA 90009-2960. It was reviewed and approved for The Aerospace Corporation by J. M. Straus, Director, Chemistry and Physics Laboratory. Lt Borden was the project officer for the Mission-Oriented Investigation and Experimentation (MOIE) Program.

This report has been reviewed by the Public Affairs Office (PAS) and is releasable to the National Technical Information Service (NTIS). At NTIS, it will be available to the general public, including foreign nationals.

This technical report has been reviewed and is approved for publication. Publication of this report does not constitute Air Force approval of the report's findings or conclusions. It is published only for the exchange and stimulation of ideas.

MARK W. BORDEN, 1ST Lt, USAF
MOIE Project Officer
SSD/MWBA

JONATHAN M. EMMES, Maj, USAF
MOIE Program Manager
AFSTC/WCO OL-AB

PREFACE

Accesion For		
NTIS CRA&I	☑	
DTIC TAB	☐	
Unannounced	☐	
Justification		
By		
Distribution /		
Availability Codes		
Dist	Avail and / or Special	
A-1		

CONTENTS

FIGURES

FIGURES (continued)

TABLE

I. INTRODUCTION

Molybdenum disulfide (MoS_2) is a useful solid lubricant because it deforms plastically more readily than the solid surfaces between which it is placed. On the macroscopic scale, the low shear strength of MoS_2 reduces the friction between sliding surfaces. On the atomic scale, the low shear strength (which results in low friction) of MoS_2 is explained by the material's anisotropic crystal structure and bonding: MoS_2 is comprised of hexagonally packed planes (a, b = 0.274 nm, c = 1.23 nm) consisting of a layer of Mo bounded on each side by a layer of S (see Fig. 1). All effective strong bonding is within the "sandwich" planes, with weaker van der Waals bondings between adjacent sandwiches. MoS_2 is strong in two dimensions and weak in the third dimension, which makes the material a two-dimensional mechanical analog to one-dimensional linear polymers. The low-shear-strength basal planes provide an atomic mechanism for single-crystal plastic deformation. This mechanism plays a role similar to that of dislocations in close-packed metals. However, on the microstructural scale, which relates atomistic phenomena to macroscopic phenomena, the mechanisms of MoS_2 plastic deformation have not been fully explained. For example, MoS_2 lubricants are polycrystalline, and while the mechanism of basal plane slip explains deformation within a single crystal, the mechanism of intercrystalline slip and its contribution to overall deformation are not understood at this time.

Sputtering provides a method of applying MoS_2 as a lubricant in thin film form; it avoids the use of organic binders used in powder applications, which can outgas in the vacuum of space. Studies have attempted to relate MoS_2 sputter-deposition conditions to the material's mechanical properties, such as friction and wear, and oxidation resistance [1-5]. However, an increasing emphasis has been placed on elucidating the physical properties of films, such as composition, crystallinity, crystal orientation, and adhesion, in order to explain the effects of deposition conditions on film performance [6-25]. These microstructural studies

7

2H–MoS$_2$

(0 0 1)

(0 1 0)

(1 0 0)

● Mo

◎ S
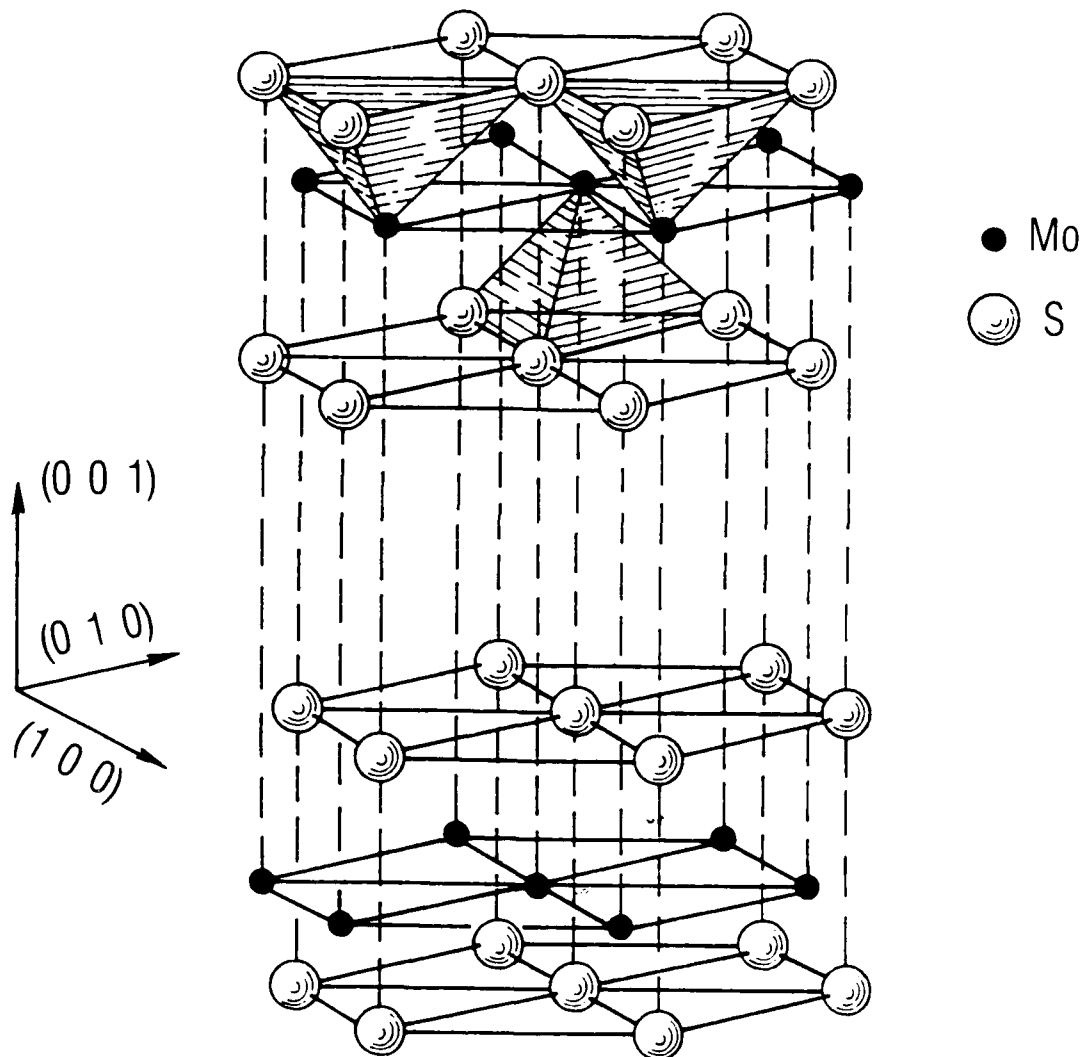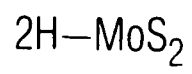
Fig. 1. The MoS$_2$ crystal structure

indicate that MoS_2 films often possess a columnar-plate, zone 2 morphology (the Thornton model [25,26]), with the basal plates perpendicular to the substrate. The zone 2 morphology is indicative of active surface diffusion during film growth, which is favored by elevated substrate temperatures (these temperatures, in turn, being influenced by secondary-electron bombardment) and, in the case of MoS_2, by a reduced water-vapor-pressure background during deposition [15,17,18].

The zone models use the dominant diffusion mechanism operating during growth as a classification criterion. The zone 1 structure is the result of a low (or absent) adatom mobility that is insufficient to overcome the effect of the shadowing favored at low T/T_m (deposition and melting temperatures, respectively) and high gas pressures. (In general, increasing gas pressure enhances the shadowing of the impinging flux, as well as decreasing the kinetic energy of ion bombardment in plasma deposition processes. Gas pressure was added by Thornton [26] to the original model of film formation via evaporation developed by Movchan and Demchishin [27] as an additional measure, along with homologous temperature, of the degree to which adatom mobility is affected by deposition conditions.) The morphology of zone 1 films consists of large dome-capped grains that have poorly defined fibrous interiors. The films can be amorphous or crystalline, they often contain voids, and they generally have poor mechanical properties. The zone 2 structure results when surface diffusion dominates; this structure consists of well-defined columnar grains that have faceted or flat tops. In most materials, the zone 2 columns are equiaxed in the directions parallel to the substrate. However, sputter-deposited MoS_2 films possess a columnar-plate zone 2 morphology, which is a consequence of the material's highly anisotropic, planar crystal structure and bonding. The MoS_2 zone 2 morphology contains porosity, which we believe is in part a consequence of the initial nature of nucleation, as discussed in Section III. The zone 3 structure occurs when lattice diffusion dominates. Grain growth or recrystallization can occur, promoting large columnar grains or equiaxed grains, respectively. The mechanical properties of zone 2 and zone 3 structures are better than those of zone 1

9

structures. Thornton also defined a zone T (transition) morphology, favored by lower gas pressures and a higher T/T_m, that was between the zone 1 and 2 structures. The zone T material has the zone 1 fibrous interior, but with flat tops; it is not porous, and its mechanical properties can be good.

The basal planes of sputter-deposited MoS_2 are believed to orient perpendicularly to the substrate because of chemically active sites on the substrate surface. These sites react more readily with the MoS_2 edge planes, such as the (100) or (110) planes, than with the (001) basal plane, which is the thermodynamically favored orientation [28]. Recently, it has been shown that MoS_2 can be deposited with the basal planes parallel to the substrate on silicon [28] and silicon carbide [29] when the substrate is heated prior to deposition. This heating presumably removes the active surface sites (such as hydroxyl groups [28]). When surface diffusion is suppressed during growth, a fibrous, equiaxed (in directions parallel to the substrate) columnar zone 1 or zone T (transition) morphology is formed. This morphology generally does not possess long-range crystallographic order [24]. A zone 1 or zone T morphology can be induced by sputter deposition at reduced temperatures [7], by reduced pressures [23], by the presence of water vapor during deposition [15], and by ion implantation of sputter-deposited films after synthesis [21,25].

During sliding wear, a deformed region, sometimes confined at the surface (Fig. 2), is formed. In this region, the basal planes in zone 2 films are reoriented parallel to the substrate, resulting in improved lubrication [24]. Films with a zone 1 (zone T) morphology can sometimes undergo a stress-induced crystallization in this deformed region. This crystallization also yields basal planes parallel to the substrate that facilitate lubrication. However, if the zone 1 films are extremely disordered when they are deposited (e.g., when deposition is conducted at liquid nitrogen temperatures), then film lubricity is very poor [7].

The structure within the MoS_2 morphology must be determined if one is to understand the mechanisms of polycrystalline film deformation and also
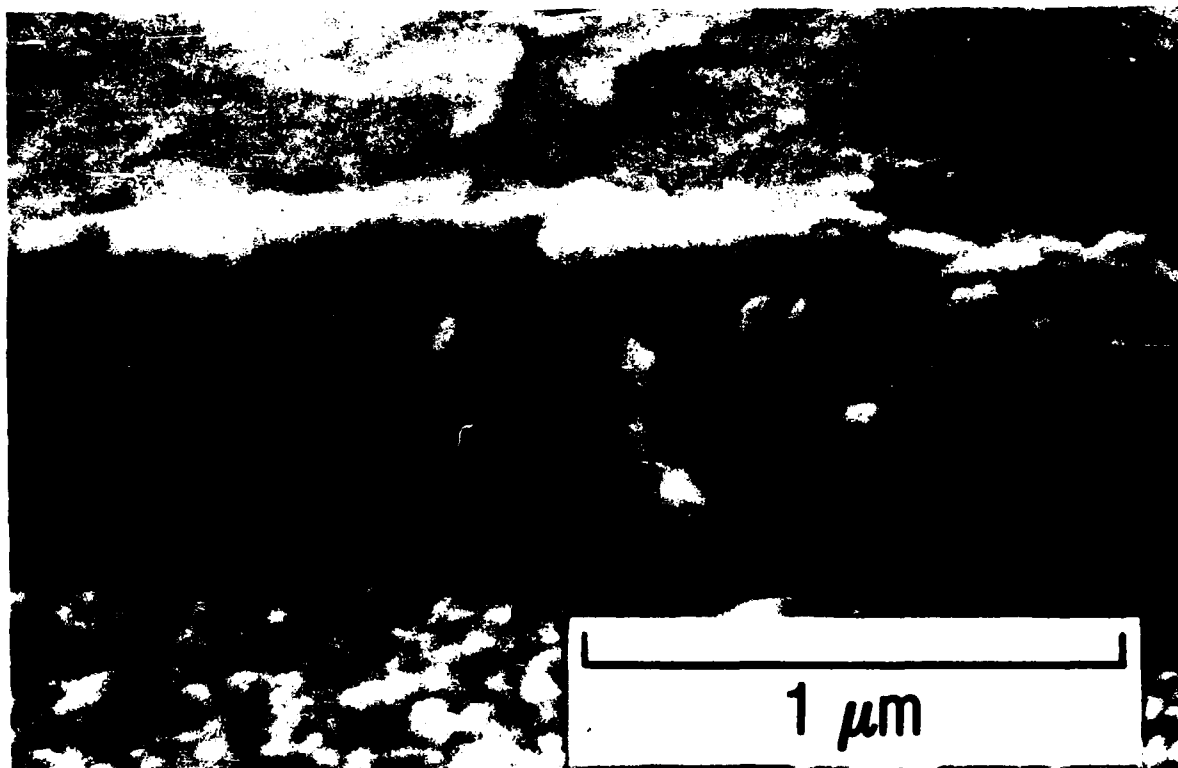
Fig. 2. SEM micrograph of a sputter-deposited MoS$_2$ film after low-load
sliding wear, showing a cross section of the deformed morphology.
A deformed region develops above the as-deposited zone 2 columnar
morphology, changing the (001) basal orientation (which shears easily
and allows lubrication) from perpendicular to parallel to the
substrate. Tilt: 30°.

of nucleation. To date, few high-resolution studies of the nanostructure of sputter-deposited MoS_2 films have been made using transmission electron microscopy (TEM). Spalvins has shown, with bright-field imaging, that film morphology changes with deposition temperature [7]. The average size of crystallites was reported to increase with deposition temperature. The estimates of crystallite size were apparently based on measurements of diffraction-ring line broadening. Other investigators have also published bright-field images and diffraction patterns [6,7,10,12,19,25,30-32].

Lattice imaging and dark-field imaging can provide spatial correlations between crystallographic and morphological structure. Only one lattice image [14] and one dark-field image [6] of sputter-deposited MoS_2 seem to have been reported. The dark-field image was of a film that did not possess long-range order but rather apparently had a zone 1 (zone T) morphology. In this report, we present detailed lattice and dark-field images of sputter-deposited MoS_2 films representing the early stages of growth under conditions that produce a zone 2 morphology.

II. EXPERIMENTAL

Films of MoS_2 were prepared by radio frequency (rf) sputtering accord-
ing to procedures described previously [22]. The substrates were amorphous
evaporated-carbon films, approximately 10 nm thick, that were floated over
distilled water onto standard copper TEM grids. The carbon-on-copper
substrates were placed onto a planar holder 36 mm from a 152-mm-diam
water-cooled target. Two shutters were then positioned over the samples.
One was a large top shutter used to precondition the target by sputter-
cleaning it for 100 min. The second shutter was smaller and was placed
directly over the samples, which allowed three different film thicknesses
to be prepared during the same deposition session. The sputter target was
mounted in the center of a 460-mm-diam bell-jar vacuum system that was
evacuated to a base pressure of 1.3×10^{-4} Pa (1×10^{-6} Torr). Sputtering
was performed with the rf planar-diode power supply set at 350 W (equiva-
lent to 1.93 W cm^{-2}) and an argon pressure of 2.66 Pa (2.0×10^{-2} Torr).

Films were prepared with substrate temperatures of 70°C (designated
AT, for ambient temperature) and 220°C (designated HT, for high tempera-
ture). Previous studies have shown that these growth conditions yield
films possessing a columnar-plate zone 2 morphology with the (001) planes
perpendicular to the substrate. The growth rates of the AT and HT films
differ, based on measurements of thick films. These rates are 0.41 and
0.58 nm/sec, respectively. The AT films were prepared with deposition
times of 22, 44, and 88 sec, which would yield respective estimated film
thicknessess of 9.0, 18, and 36 nm. The HT films were prepared with
deposition times of 20, 40, and 70 sec, yielding respective estimated film
thicknesses of 11, 23, and 40 nm. It must be emphasized, however, that the
exact time at which deposition is initiated is uncertain. Thus, time
comparisons between AT and HT films should be viewed with some caution,
since (1) the films were prepared in separate sessions, (2) the total
deposition times are short relative to the uncertainty of the initiation
time, and (3) the thicknesses are based on growth rates determined from
thicker films.

By means of a Phillips model CM 10 TEM with a beam voltage of 80 keV,
the films were initially screened for suitability in the bright-field
mode. Subsequent analyses were performed by means of a Phillips model EM
420 scanning transmission electron microscope (STEM with a beam voltage of
120 keV, used primarily in the TEM mode. Lattice images of the (002) basal
plane were obtained. Dark-field images were obtained from arcs of the
(002) basal-plane (100) and (110) edge-plane diffraction rings, and
diffraction patterns were also recorded. An evaporated-aluminum film on
carbon was used to calibrate the camera length, and a graphite standard was
used to calibrate the magnification.

III. RESULTS AND DISCUSSION

A. THE NANOSTRUCTURE OF EARLY-GROWTH FILMS

All the samples examined were found to be suitable for TEM analysis, insofar as they were thin enough to allow the electron beam to penetrate them. The technique of increasing the deposition time to investigate morphology reveals that early-growth morphology consists of anisotropic, acicular islands. The micrographs show that the lattice fringes corresponding to the (002) basal plane are oriented perpendicularly to the substrate and along the major axis of the islands. These images agree with an image published by Bichsel et al. [14]. Figures 3a-c show that the areal density, length, and width of the MoS_2 islands increase with deposition time. This observation of island nucleation and growth provides insight as to why the surface chemistry observed by electron energy-loss spectroscopy (EELS) on films grown under similar conditions (but on silicon substrates [33]) appears very complex; i.e., MoS_2 nucleation and vertical growth are heterogeneous on the substrate. This nanostructure has been observed by many investigators using bright-field imaging [6,7,10,12,19, 25,30-32].

Selected-area electron diffraction (SAED) patterns representative of HT and AT films are shown in Figs. 4 and 5. The (002) basal plane and (100) and (110) edge plane reflections of the hexagonal crystal structure are present. As stated earlier, the presence of the (002) reflection indicates that the basal planes are most likely perpendicular to the substrate. Dark-field imaging using arcs of the (002) ring shows, in Fig. 6, that the basal plane orientation is associated with the island structures, in agreement with the lattice image data. Dark-field imaging using either the (100) or (110) reflections indicates that the diffracting regions are more uniformly distributed (Fig. 6c-d). The presence of (100) and (110) reflections outside of the islands suggests that there is a heterogeneous distribution of regions whose basal plane orientation is essentially parallel to the substrate, adjacent to the acicular islands.
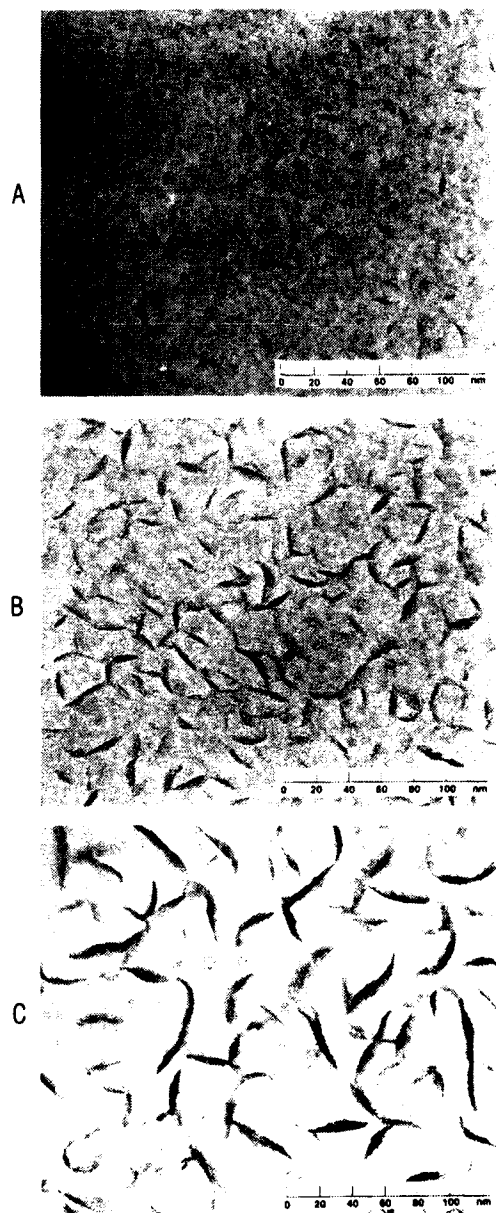
Fig. 3.   TEM lattice images of the (002) basal planes of MoS_2 HT (see text)
          films on carbon, showing that the early nucleation morphology
          contains anisotropic islands. The (002) planes are perpendicular to
          the substrate and along the major axis of the islands. These nuclei
          are classified as "edge islands" because edge facets are parallel to
          the substrate. Rapid growth occurs along the edge planes and is
          shown as function of deposition time. Estimated thickness: (A)
          11 nm, (B) 23 nm, (C) 40 nm. Basal islands with (001) planes
          parallel to the surface exist between the edge islands (see Fig. 6).
          The edge islands quickly shadow and inhibit further basal island
          growth.
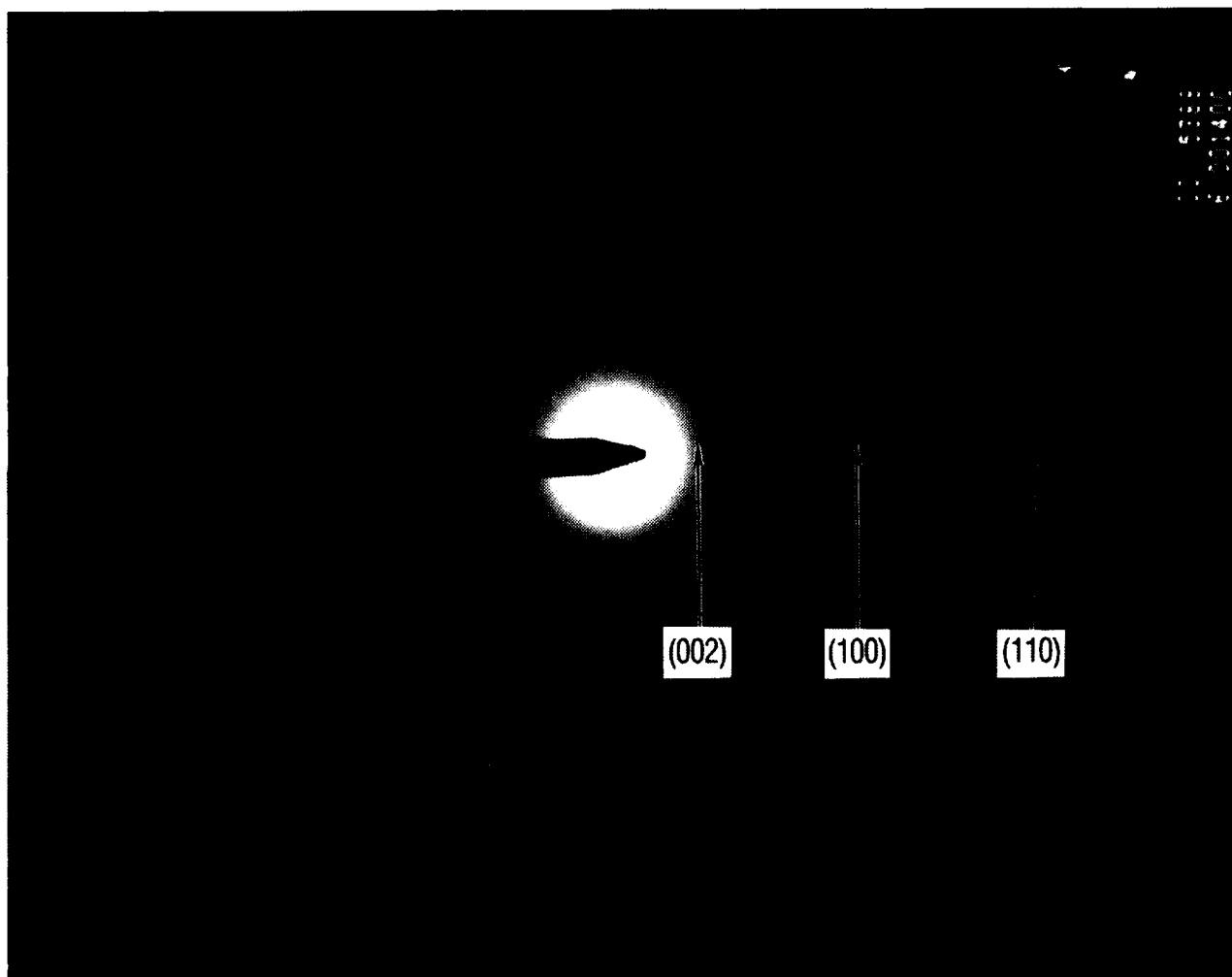
Fig. 4. Diffraction pattern of an HT MoS$_2$ film. Estimated thickness: 40 nm.
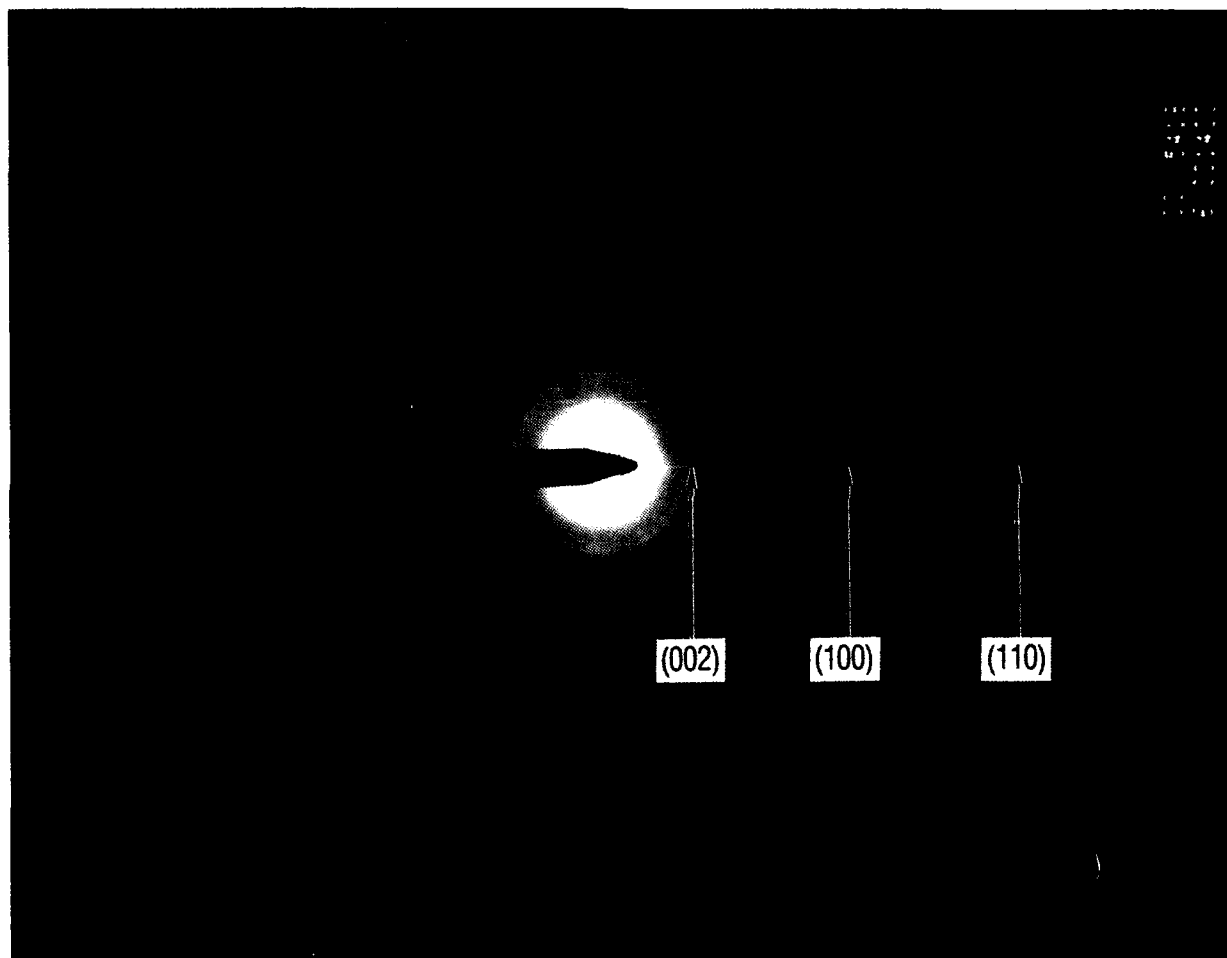
Fig. 5. Diffraction pattern of an AT MoS$_2$ film. Estimated thickness: 36 nm.
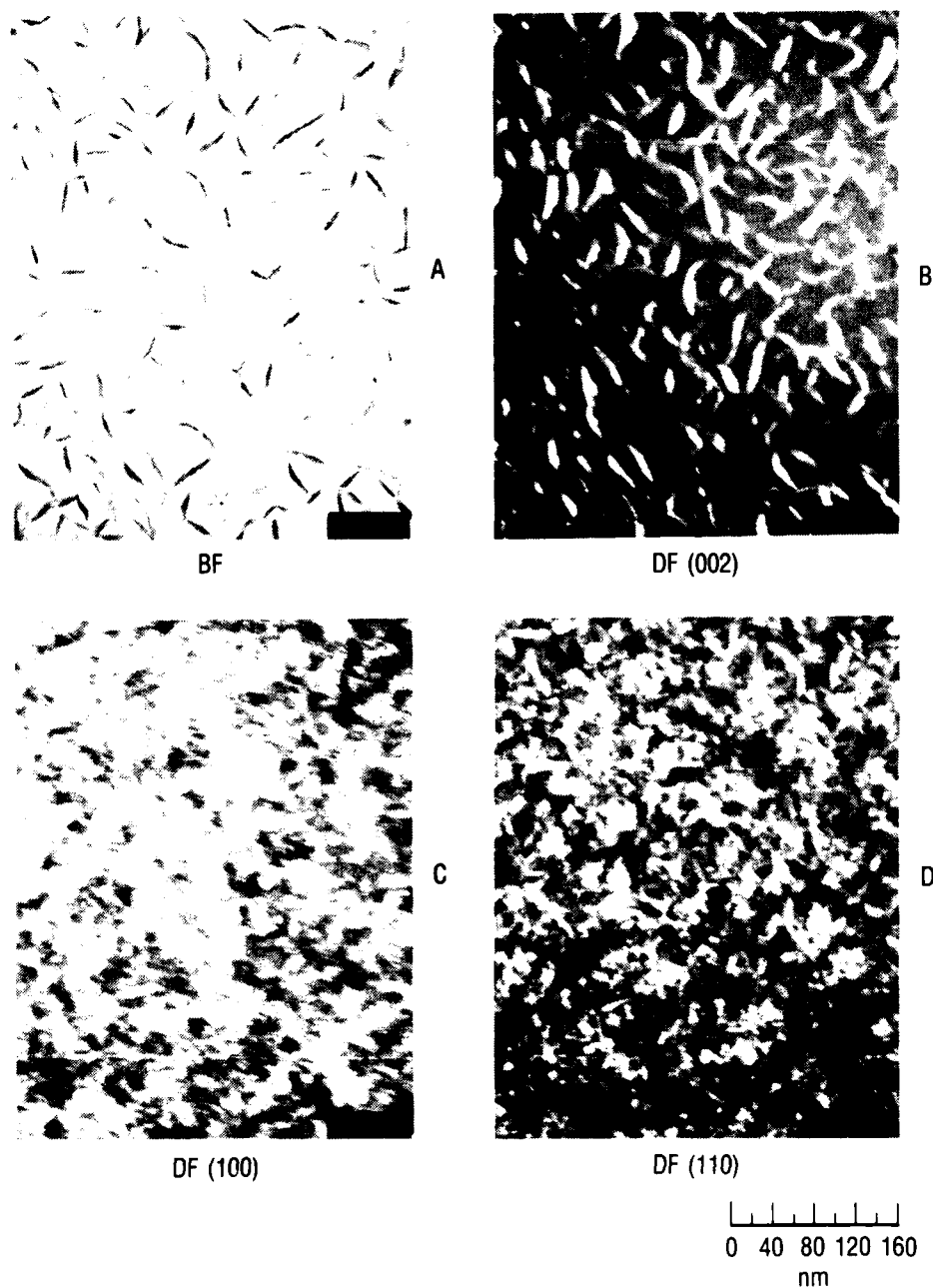
Fig. 6. (A) Bright-field (BF) image of an HT MoS_2 film (estimated thickness: 40 nm), (B) a corresponding (002) dark-field (DF) image, (C) a (100) dark-field image, and (D) a (110) dark-field image. The images show that basal orientation <u>perpendicular</u> to the substrate is confined in the acicular edge islands (this agrees with the lattice images in Fig. 3), and that edge-plane orientation perpendicular to the substrate is more widespread, indicating the existence of "basal islands," in which the (001) basal orientation is <u>parallel</u> to the substrate, between the edge islands (see text).

Energy dispersive spectroscopy (EDS) data obtained by using the small-spot (approximately 50 Å) STEM mode indicates that Mo and S are present between the acicular islands, although they do not necessarily represent stoichiometric MoS_2. An examination of lattice images as a function of sample tilt (0-45°) shows that the islands, tilted out of the interference condition, assume a moderate-gray to dark-gray appearance (Fig. 7). Such regions are present in many areas at zero tilt, suggesting that MoS_2 is present in those areas where the basal planes are at an acute angle to the substrate surface. Occasionally some lattice images appeared at increasing tilt, which also confirms this interpretation.

The dark-field and lattice image data show that two general types of MoS_2 nuclei are present in the early-growth nanostructure, one whose basal planes are perpendicular to the substrate, exposing edge-plane surfaces, and the other whose basal planes are essentially parallel to the substrate, exposing the basal plane surfaces. For the remainder of this report these types will be referred to as "edge islands" and "basal islands," respectively. These appear to be the two general types of orientation, although the data on lattice image tilt indicate that some islands have an orientation between these two limiting cases. Within the context of the active-sites nucleation model [28,33], the TEM data show that localized regions of the substrate in an early-growth, zone 2 morphology can lack the active sites needed to induce edge orientation. This model differs slightly from the original model, which assumed that only edge islands or only basal islands were present.

The orientation and the anisotropic shape of the edge islands indicate that MoS_2 crystals grow faster in the edge directions than in the basal direction. Growth in the edge direction along the substrate surface appears to be stopped by the impingement of the islands. This growth pattern is reasonable from a chemical viewpoint, because the edge surfaces of MoS_2 are more reactive than the basal surface. Furthermore, lamellar edge growth is favored from the standpoint of diffusion. Since S and Mo planes are exposed, a mobile adatom on an edge surface can readily diffuse and attach onto a proper site. On the other hand, growth in the basal

20

0°
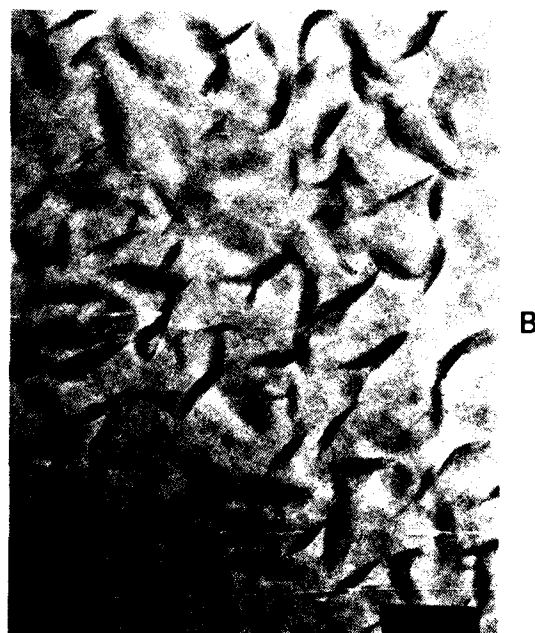
45°

0 20 40 60 80 100
nm

Fig. 7.   Basal plane (002) lattice images as a function of sample tilt,
          showing that the edge islands develop the dull gray appearance of
          basal islands when viewed outside of the lattice imaging condition.
          (A) 0°, (B) 45°. Sample: HT. Deposition time: 70 sec.

direction requires the sequential addition of an appropriate adatom species, which is a more complicated (and kinetically slower) process.

The localized edge islands merge and evolve into the zone 2 columnar plate morphology (Fig. 8). This morphology presumably dominates because growth rates are faster here than they are in the basal morphology, which is ultimately shadowed and covered. The presence of basal islands in the early-growth structure induces subsequent film porosity. This dominance of edge-island growth reinforces the idea that active sites on the substrate surface must be eliminated prior to deposition, to allow continued basal island growth to occur. Conversely, active sites on the substrate surface should be promoted to favor a dense edge island structure, and hence low porosity film, to evolve.

The AT morphology and growth sequence appear similar to the morphology and growth of the HT films. A lattice image of a 36 nm AT film appears in Fig. 9. The edge island density of the AT film seems to be greater than it is in the HT film, but the island dimensions in both films are similar. In both cases, island length in the edge direction along the substrate surface ranges from 20 to 40 nm, while island width in the basal direction ranges from 4 to 8 nm. A similar correspondence in size was also observed between AT and HT films having shorter deposition times. However, as thickness increases, a disparity in edge plate density and dimensions develops between the AT and HT films (Fig. 10), although the plate dimensions at the surface in both types of thicker film are larger than the edge island dimensions near the interface. This is because film structure is dependent upon adatom mobility. These edge-island-size results indicate that substrate surface-chemical effects strongly influence film nanostructure in the early stages of film growth, presumably through their influence on mobility. Once the substrate is effectively covered, substrate temperature becomes the dominant influence in subsequent film growth.

A careful analysis of the dark-field images indicates that the edge islands possess (100) and (110) orientation <u>perpendicular</u> to the substrate and perpendicular to the basal planes. This suggests that two types of
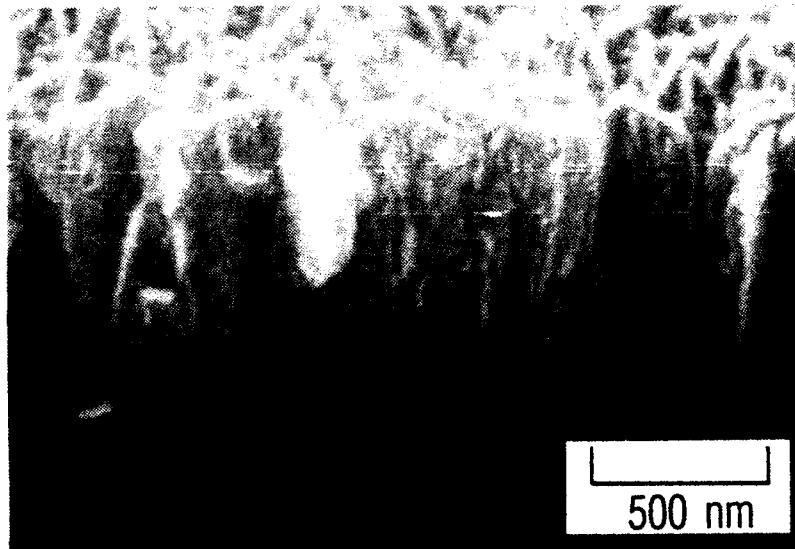
Fig. 8. SEM cross-sectional view of a thick MoS$_2$ film showing the evolution of the zone 2 columnar-plate microstructure that develops from the interface region. Tilt: 30°.
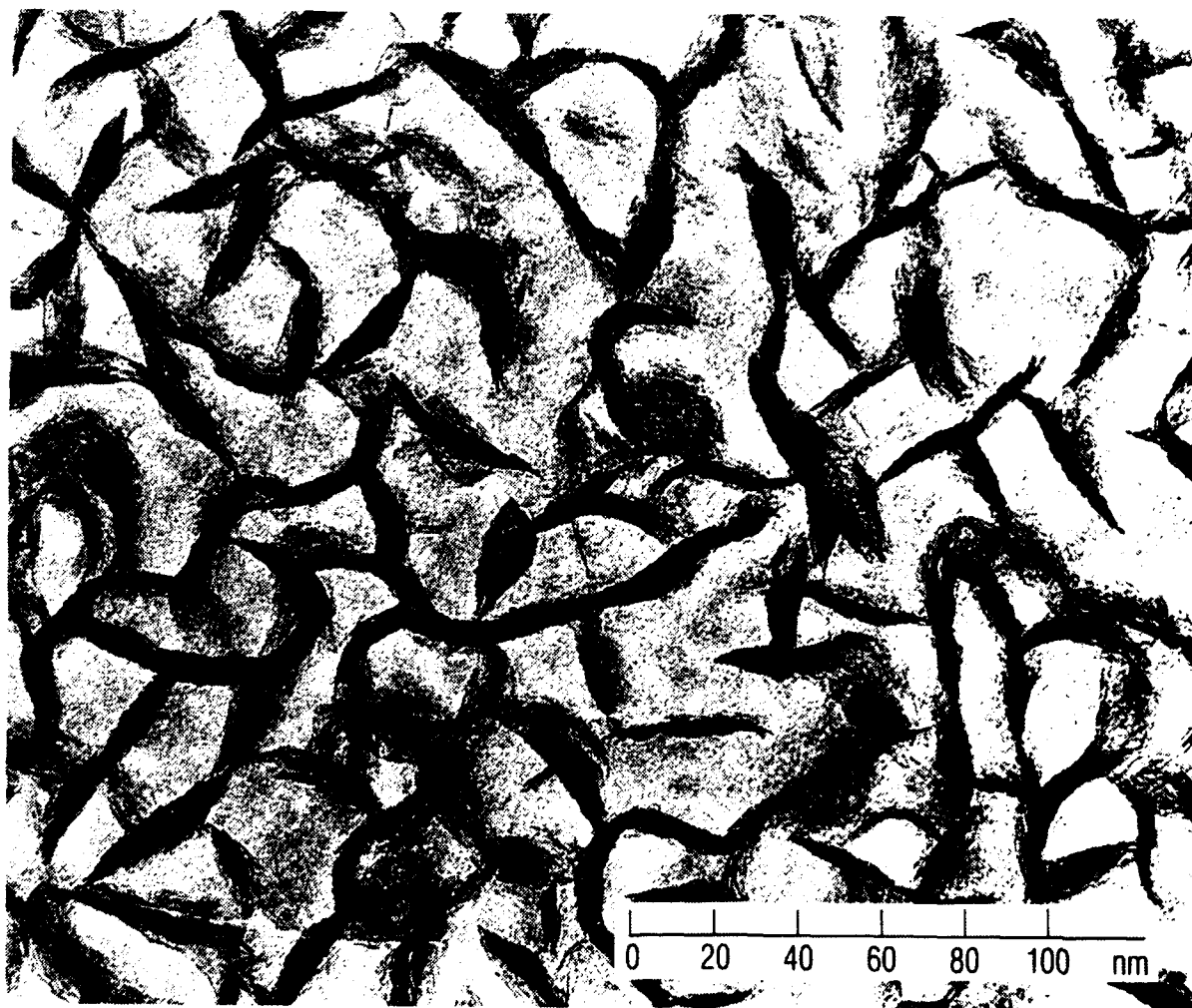
Fig. 9. TEM basal plane (002) lattice image of an AT (70°C) MoS$_2$ film
(estimated thickness: 36 nm), which reveals a nanostructure similar
to that of the HT film shown in Fig. 3c.
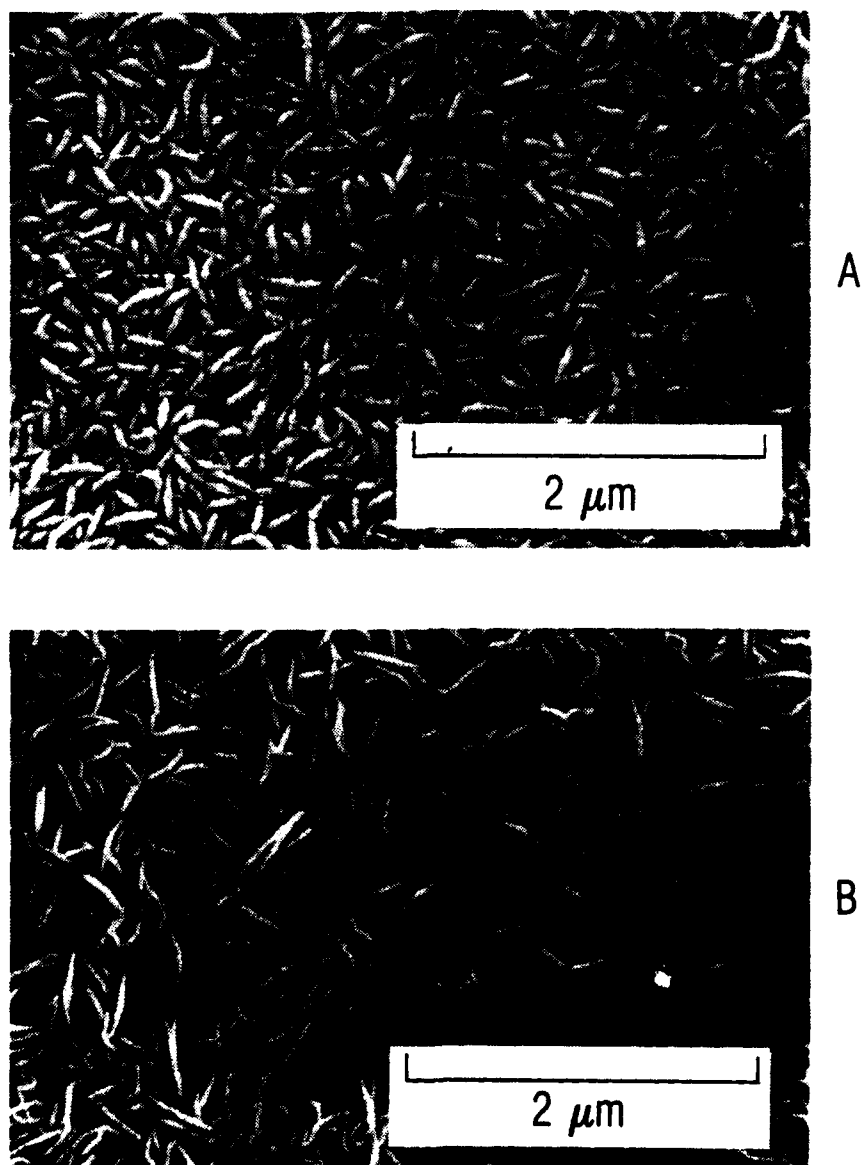
Fig. 10. SEM micrographs of the surface morphology of thick MoS_2 AT (A) and HT (B) films. The AT film has a denser morphology and smaller plate length than the HT film, while the nanostructures near the interface were very similar (compare Figs. 3c and 9), suggesting that the interface strongly affects adatom mobility in the early stages of growth.

edge islands are present, whose surface orientations <u>parallel</u> to the substrate are different. If an edge island nucleates with the (100) plane parallel to the surface, horizontal growth is fast in the [010] and [0$\bar{1}$0] directions and slow in the [001] and [00$\bar{1}$] basal directions, while vertical growth is fast in the [120] direction. Nucleation with a (110) plane parallel to the surface will yield fast horizontal growth in the [1$\bar{1}$0] and [$\bar{1}$10] edge directions, slow horizontal growth in the [001] and [00$\bar{1}$] basal directions, and fast vertical growth in the [110] edge direction.

X-ray diffraction (XRD) experiments on thicker (0.5 μm or greater) films indicate that the (100) parallel orientation dominates on steel substrates from ambient temperature to 220°C [22]. At 320°C, the percentage of (110) orientation is greater than at lower temperatures. The dark-field results indicate that both orientations are present near the surface, suggesting that the (100) parallel orientation subsequently grows faster than the (110) orientation at temperatures up to 240°C. The initial presence of either edge orientation is probably controlled by local nucleation conditions on the surface, while the dominance of one orientation over the other in thicker films is controlled by growth kinetics.

It is worth reemphasizing here that the scattering vector $\bar{G}$ (the vector subtraction of the incident-beam vector from the diffracted-beam vector) differs for SAED and XRD when the same material is observed. In SAED, $\bar{G}$ lies essentially in a plane parallel to the substrate (Fig. 11a). In XRD, for the diffractometer case, $\bar{G}$ is perpendicular to the substrate, sampling all lattice planes parallel to the substrate (Fig. 11b). For the MoS_2 samples in the edge island regions presented in this report, SAED will detect a basal reflection, while XRD will not. This is because the basal planes are perpendicular to the surface. SAED will also detect an edge reflection, because the crystal structure of MoS_2 requires that if basal planes are perpendicular to the substrate, some edge planes must also be perpendicular to the substrate. Furthermore, because of the crystal structure of MoS_2 and the diffraction-orientation relationship between SAED and XRD, an edge island that yields a (100) reflection in SAED will yield a (110) reflection in XRD, as shown in Fig. 11c. Accordingly, if a (110)
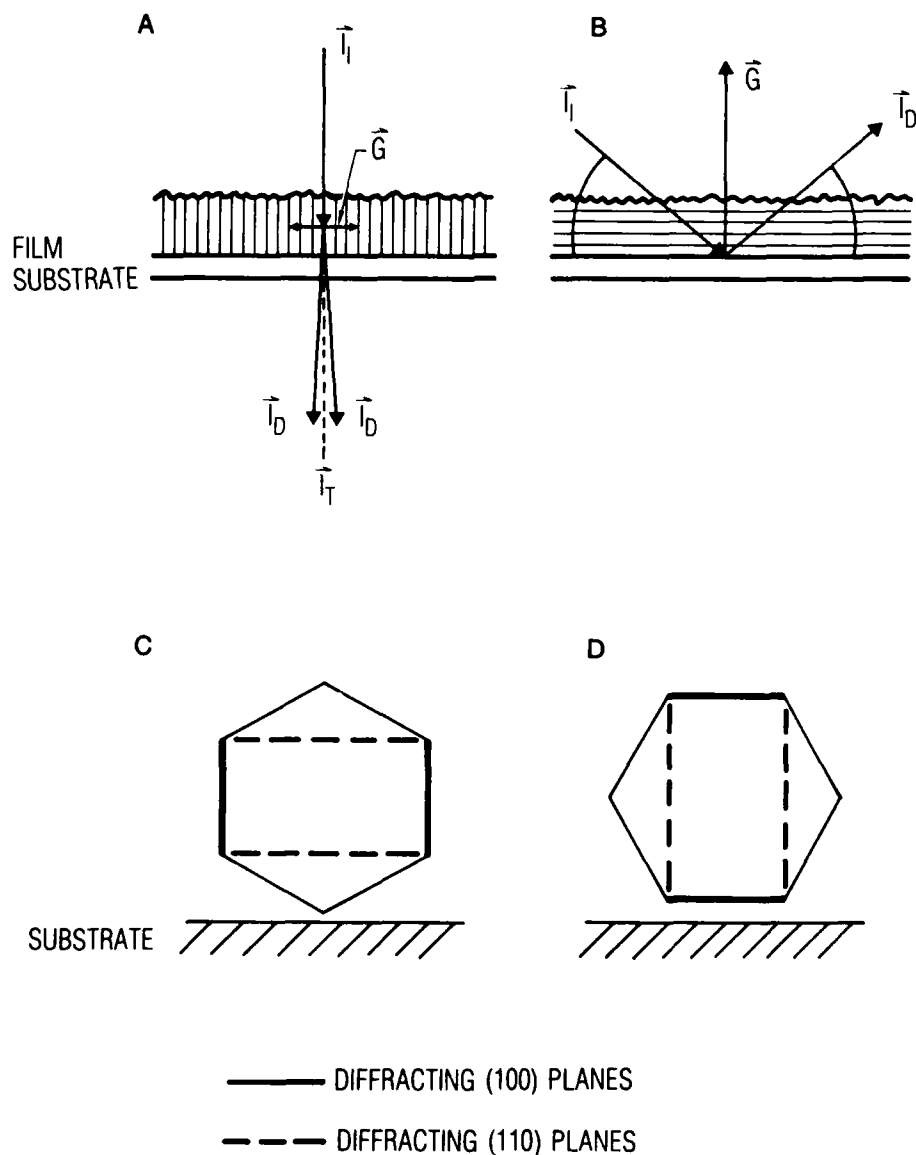
Fig. 11. Schematic drawings showing the geometric relationships between the diffraction methods used in this study and the film's crystal structure. (A) The diffraction geometry for SAED, where planes are perpendicular to the substrate diffract. (B) The diffraction geometry for XRD, where planes are parallel to the surface diffract. (C,D) Hexagons representing either the Mo or the S sublattices in an edge island above the substrate: (C) (002) and (100) planes diffract in SAED, and (110) planes diffract in XRD; (D) (002) and (110) planes diffract in SAED, and (100) planes diffract in XRD. See Fig. 1 for the complete MoS$_2$ crystal structure.

reflection is observed in SAED, a (100) reflection will be observed in XRD, as shown in Fig. 11d.

The calculated lattice spacings of the planes observed by SAED of the sputtered MoS_2 films are listed in Table 1, along with ASTM data for single-crystal MoS_2. Relative to the standard, the (100) and (110) planes are contracted, while the basal plane spacing is dilated. These results are consistent with previous XRD measurements of thicker films prepared under similar conditions observed both as-deposited and after sliding wear. The deformation induced crystallite reorientation, so that the basal planes were then parallel to the substrate and would give rise to an (002) peak in XRD [20,22]. X-ray photoelectron spectroscopy (XPS) studies of films grown under these conditions indicate that the films contain from 5 to 15% substitutional oxygen (i.e., in the MoS_2 crystal structure or phase and not as MoO_3) and that they can be sulfur deficient [34]. Both the presence of oxygen in the $MoS_{2-x}O_x$ phase and the deficiency of sulfur are believed to cause the lattice to contract in the direction perpendicular to the (hk0) planes and to expand in the direction perpendicular to the (001) planes. With the use of molecular orbital concepts discussed in detail elsewhere [35,36], this phenomenon has been explained in terms of changes in electron distribution around the Mo atom.

Table 1. MoS_2 Film Lattice Spacings, in nm, Calculated from SAED Data

	Plane		
	(002)	(100)	(110)
AT Film	0.699	0.261	0.151
HT Film	0.690-0.707	0.261	0.152
Molybdenite [37]	0.615	0.2737	0.1581

To estimate crystallite size, the intensity profiles of the diffraction rings were analyzed by means of Scherrer's equation [38], which was the only method used in earlier TEM investigations [7]. Estimated crystallite size varied with the ring examined, and the following values were obtained: 3 to 4 nm for the (002) ring (AT and HT, respectively); 6 nm for the (100) ring (both AT and HT); and 5 nm for the (110) ring (both AT and HT). These different sizes are reasonable, since the morphology is clearly anisotropic. Although these values agree with those reported in a previous study [7], the author of that study did not specify the rings used for the estimates. However, estimates based on Scherrer's equation should be viewed with caution, because this equation ignores the broadening that originates from nonuniform microstrain [which in the present context could originate from heterogeneous distributions of point imperfections, such as vacancies, impurities (e.g., oxygen), and stacking faults]. Dark-field microscopy is a better approach. Nonetheless, the calculated values agree with the lattice image and dark-field data, which show that the near-interface nanostructures of the AT and HT films are similar. This supports the hypothesis that the substrate surface strongly affects adatom mobility in the early stages of film growth.

B.   LATTICE IMAGES

The lattice images presented in Figs. 3 and 9 show that the edge island structures are highly crystalline, with a strong basal plane orientation perpendicular to the substrate. An important question regarding the intercrystalline aspects of film lubrication is whether the edge islands should be considered as single crystals containing defects such as curvature or twisting, or as overlapping straight crystals. However, interpreting the internal structure of plates on the basis of lattice images is difficult. The lattice image is an effect of phase contrast and so is sensitive to point-to-point variations in the projected specimen's electrostatic potential [39-41]. Thickness variations and crystal overlap, as well as other factors such as the microscope's imaging conditions, can affect the lattice image. A comparison of experimental data with image simulations is required to account for these factors.

Several interesting features can be observed in the experimental data. For example, the lattice images are seldom linear throughout a MoS_2 plate. Features such as sharp displacements (Fig. 12) or fringes are present, which either may be due to local changes in thickness and/or orientation (i.e., stacking faults). Kinks in the lattice image (Fig. 13a,b) suggest discontinuous changes in crystal orientation, while curvature in the lattice image suggests a more continuous change (Fig. 14). Curvature similar to that reported here is rare, having been seen in some forms of carbon [42] and in some minerals [43]. Generally, the crystal structure of these materials is anisotropic, as it is in MoS_2. Lattice image curvature has been observed in studies of MoS_2-based catalysts [44-46]. Recently, Takahashi has observed lattice image kinking, curvature, and displacement in MoS_2 flakes that had been microtomed [47]. He interpreted the kinking and bending to represent localized fracture and deformation of the crystal, although he did not perform image simulations. The bending of MoS_2 planes has also been observed with SEM when single-crystal molybdenite has been subjected to a mode-I compressive stress [48,49]. This bending emphasizes the fact that MoS_2 is strongly bound chemically in two dimensions but weakly bound in the third dimension.

The ability of MoS_2 to bend is probably important when the material deforms as a solid lubricant. Larger MoS_2 plates have been observed with SEM to bend after shear loading [24], which is a way in which a lubricating film can be formed. In addition, bending may facilitate the formation of highly deformed surface layers that can develop during low-load sliding (Fig. 2) [11,24], and it may also be important during the final stages of film wear. It has been observed that the major portion of a sputter-deposited MoS_2 film above a critical thickness (approximately 300-400 nm) is ejected after plate fracture and that reorientation occurs early in sliding wear life [10,22]. The remaining film apparently provides the wear protection during most of component life.

The structure of this remnant film is not known. One possibility, for which we have no confirming evidence, is that the remnant plates bend, rather than fracture, below some critical plate height. The bottom of the
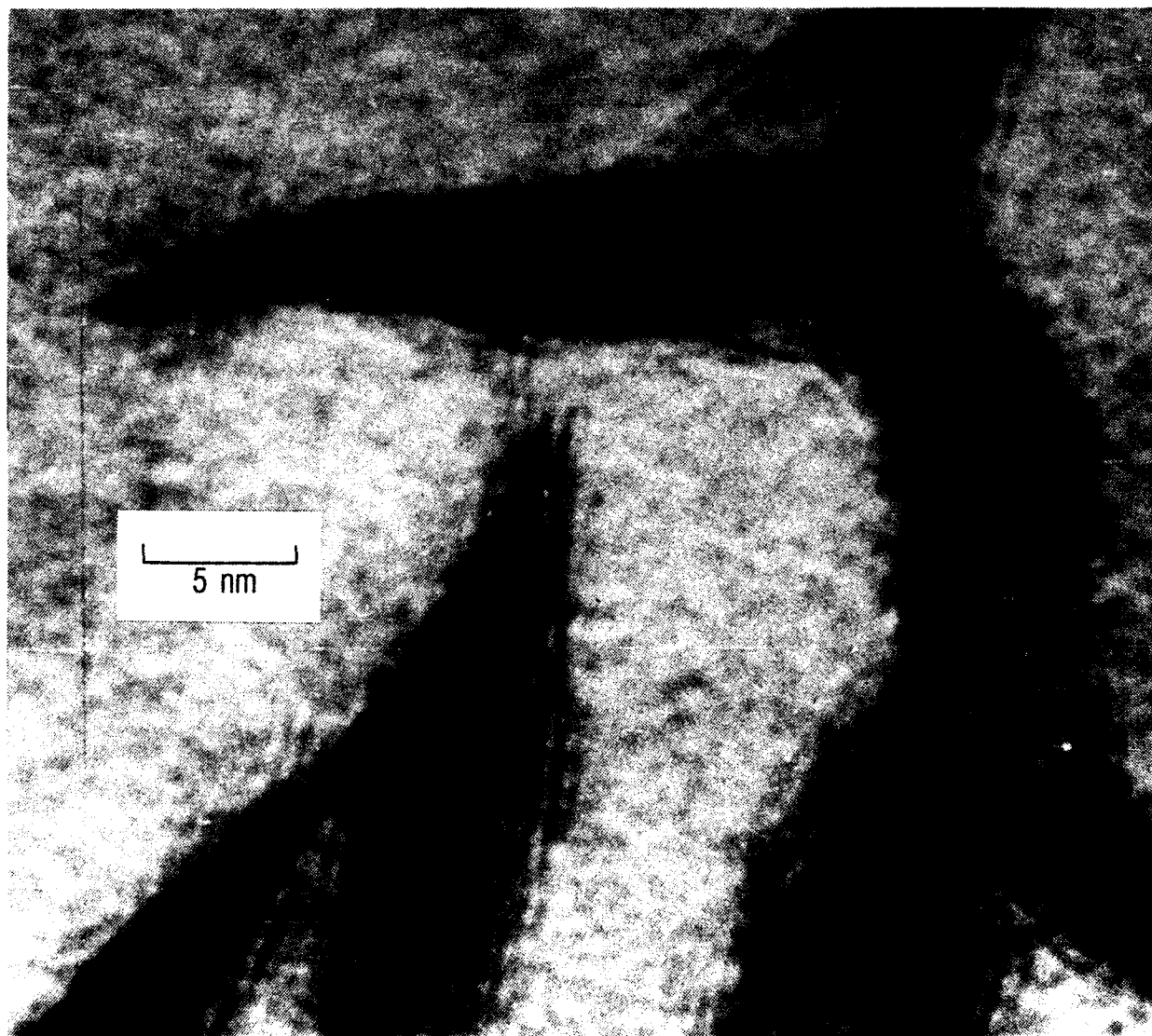
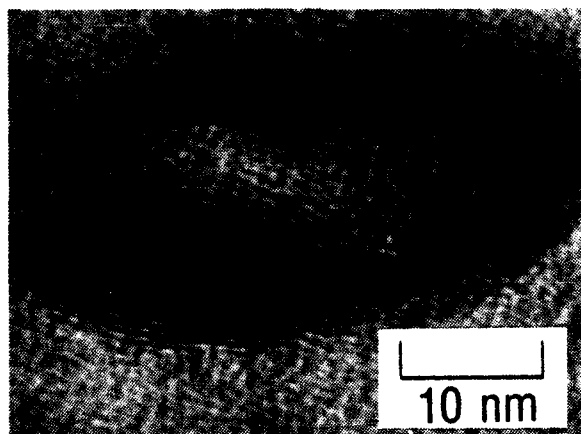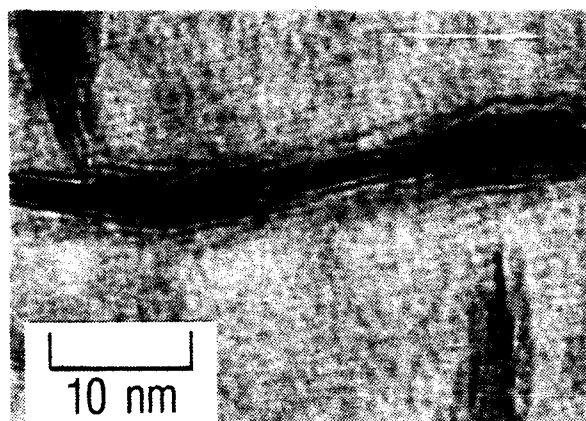Fig. 12. Basal plane (002) lattice image, showing fringe displacement and curvature

Fig. 13. Basal plane (002) lattice images, showing fringe kinking
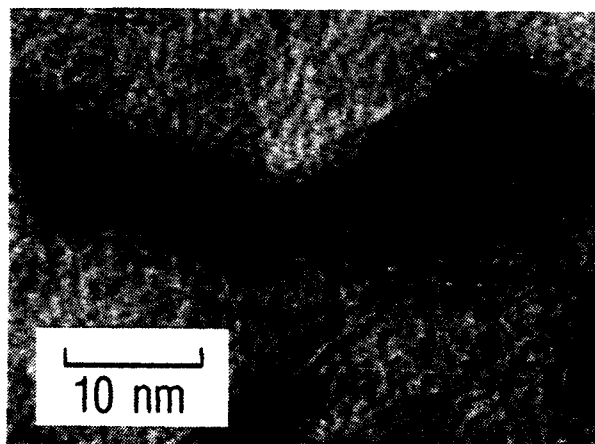
Fig. 14. Basal plane (002) lattice image, showing fringe curvature

plates could remain securely attached to the substrate because they bond strongly with the MoS_2 edge facet. The sides of the plates would thus be the exposed top of the remnant film, providing basal surfaces for lubrication. The deformed nanostructure would resemble a foil bearing. The regions between the edge oriented plates already have basal oriented material near the substrate, from the early stages of growth. This material may contribute to lubrication at the final stages of wear. A related possibility is that loose basal oriented plates may compact between the edge oriented plates.

If the lattice image curvature reported here represents basal plane bending, then some local variation in the growth process must have occurred. Evidence for this is seen in the way that the lattice fringes of some plates merge smoothly and continuously (Fig. 15), while those of other plates appear to impinge and overlap, yielding a composite moire fringe (Fig. 16). In addition to the curvature of basal planes perpendicular to the surface, the basal planes may twist out of the perpendicular. This curvature and twisting during film growth may contribute to the formation of dendrite-like side plates that are sometimes observed on the columnar plate structure.

The possible occurrence of localized curvature and twisting during later film growth could also contribute to the eventual development of edge orientation. Edge orientation has been observed in thicker films (1000 nm) grown under conditions that yield basal orientation exclusively near the interface (within 200 nm) [28,29]. In other words, even if the removal of active sites on the substrate allowed basal orientation to dominate near the interface, local variations or disturbances of growth could create regions of edge orientation during later film deposition. Thus, while interface preparation is essential to prevent edge islands from forming during early film growth, deposition conditions should probably be closely controlled in later film growth to prevent subsequent edge island formation. Conditions that favor epitaxy, such as higher surface temperatures and lower-deposition flux rates (provided that background water pressures are low enough to prevent oxygen incorporation [15,17,18]) should favor
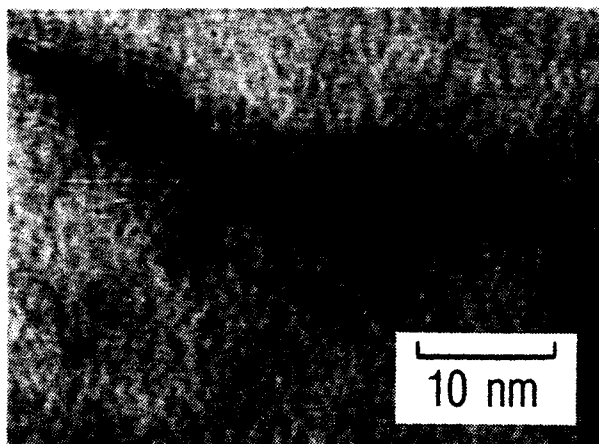
Fig. 15. Basal plane (002) lattice image, showing fringe curvature and
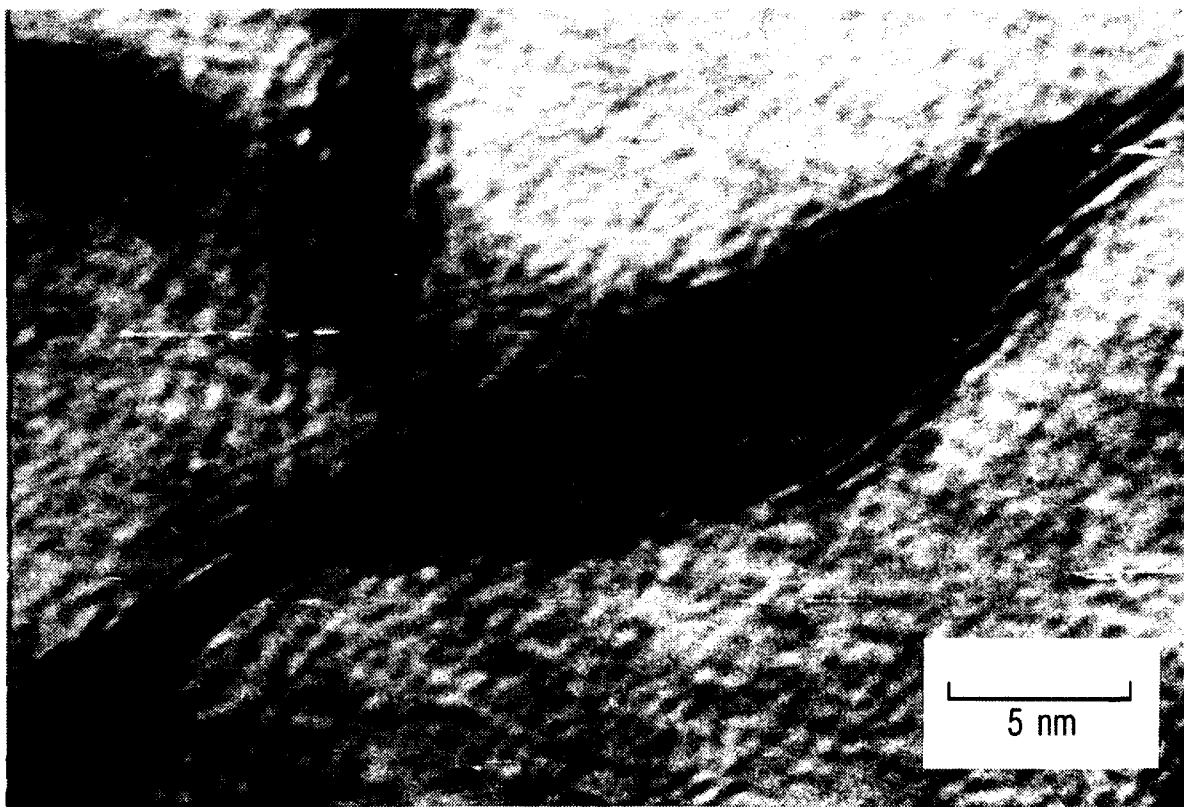merger, and suggesting that local variations in the growth process
occurred

Fig. 16. Basal plane (002) lattice image, showing a composite Moiré fringe

continued basal growth by promoting the formation of stable surfaces that have minimal defects.

Dark-field imaging reveals a variation of intensity within a single edge-island plate (Figs. 6b, 17, 18). Variations in platelet thickness, crystalline orientation, or crystalline order could cause this contrast effect. A close examination of lattice fringes as a function of tilt indicates that aligned crystallite overlap may be present, in addition to the interfering overlap that produces a moiré fringe. These results, along with the observation of curved lattice fringes, can be interpreted structurally in three ways: (1) The edge islands contain regions of differing crystallinity where order and disorder coexist, (2) the edge islands are composed of small straight crystallites that overlap (the overlap yields fringe curvature in projection), or (3) the edge islands are imperfect crystals of aligned basal planes that can easily bend or kink as a result of local growth conditions (or deformation and fracture). Model 1 can be rejected because lattice images are present throughout islands that have variable dark-field intensity. If a region were disordered, no lattice image should appear in that area. The dark-field intensity variations and the tilted lattice images do not conclusively distinguish between models 2 and 3. However, given the fact that MoS_2 basal planes will continuously bend under compressive stress, and the fact that curved lattice images are generally associated with anisotropic materials, model 3 seems reasonable. Higher voltage TEM studies, which could more effectively use higher order MoS_2 diffraction rings to form lattice images, would help to clarify this issue, as would image simulation.

C. FILM OXIDATION/DEGRADATION

MoS_2 is thermodynamically unstable with respect to MoO_3 formation [50]. Previous studies have shown that sputter-deposited films oxidize on the surface, over a period of months [12]. It was found that within 6 months of preparation, the thinner AT films underwent a morphology change, as shown in Fig. 19. The acicular-edge island morphology was initially unstable under the electron beam. When a new region was examined, signifi-

RF (AT)

A

B
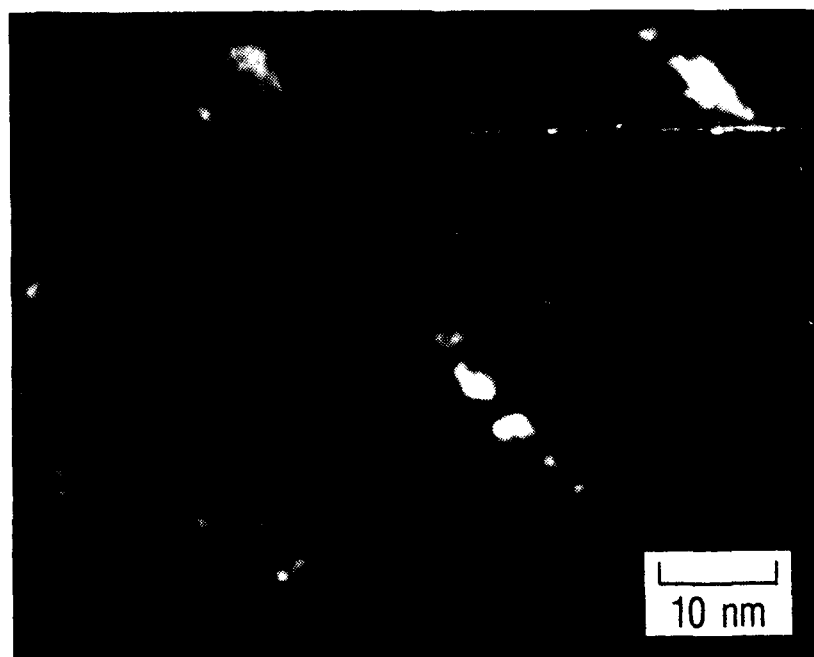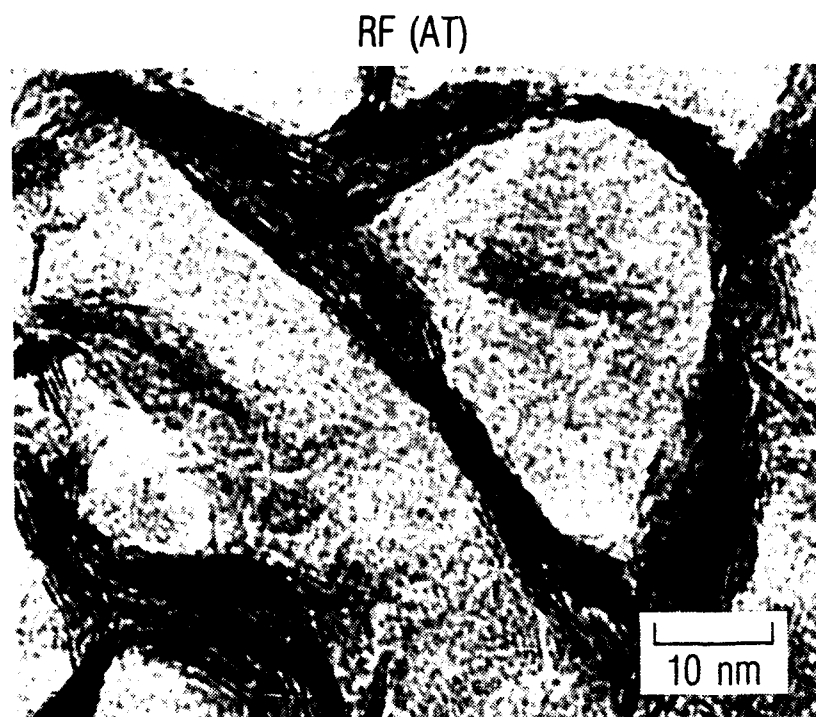
Fig. 17. AT film, exhibiting (A) a basal plane (002) lattice image with (B) a corresponding (002) dark-field image, showing that the edge islands are not perfectly straight single crystals; some deviation is present.

RF (HT)

A
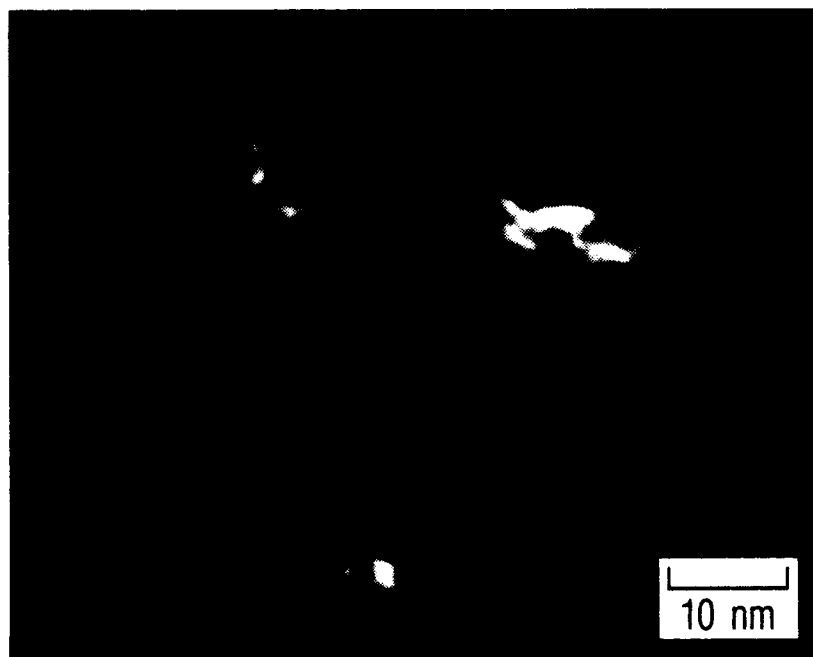
B

Fig. 18. HT film, exhibiting (A) a basal plane (002) lattice image with (B) a
corresponding (002) dark-field image, showing that the edge islands
are not perfectly straight single crystals; some deviation is
present.
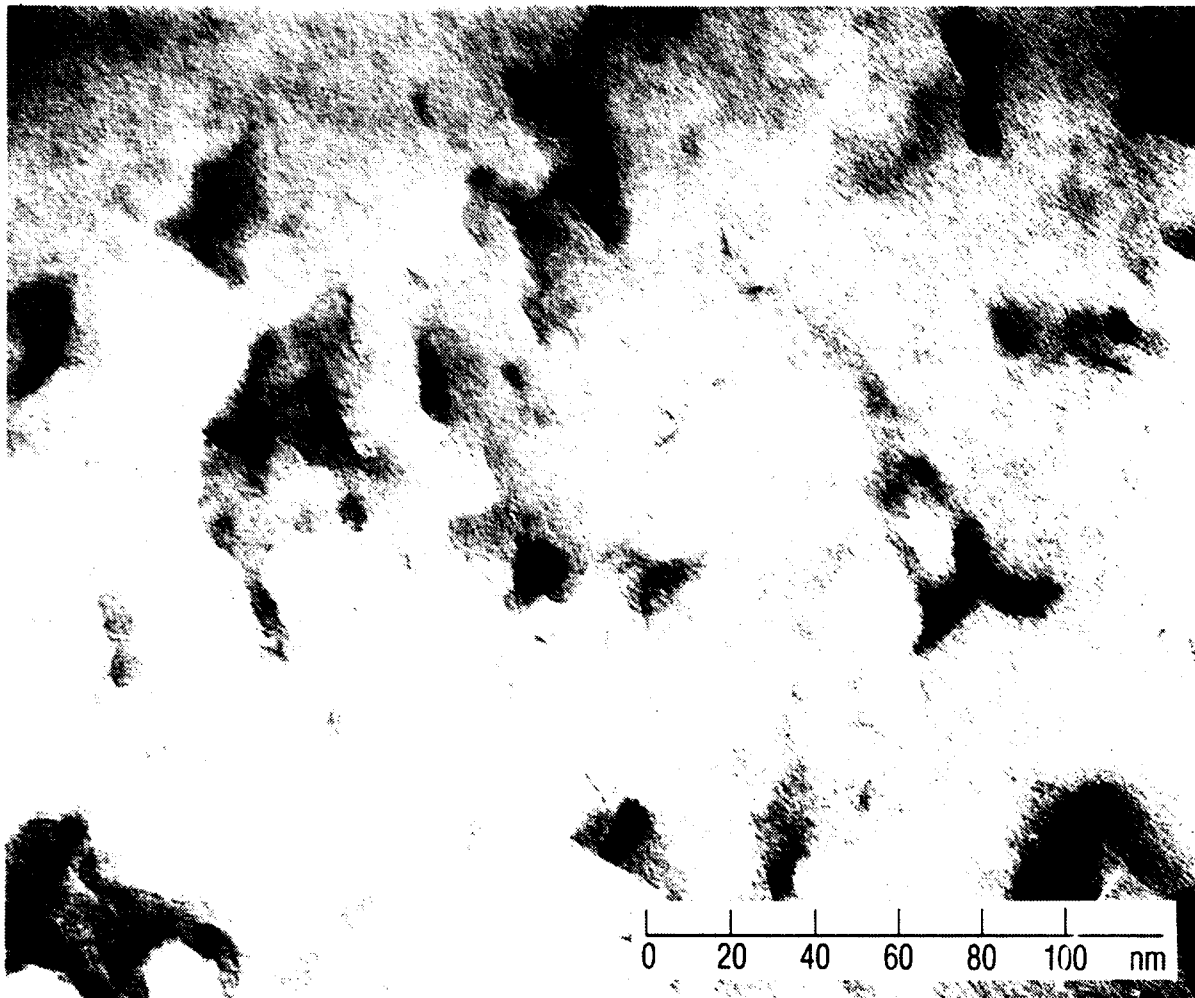
Fig. 19. TEM micrograph, exhibiting the morphology degradation (presumably oxidation) that occurred in the sample shown in Fig. 3a after 8 months.

cant outgassing, as evidenced by sample motion (rupture), occurred for about 10 sec. SAED revealed new diffraction rings with d-spacings of 0.30, 0.24, 0.14, and 0.12 nm. The thinner HT films developed a similar structure within 8 months, with TED spacings of 0.33, 0.20, and 0.17 nm. Although MoO_3 has some corresponding spacings (d_{210} = 0.345, d_{300} = 0.304, d_{410} = 0.199, and d_{420} = 0.1724 nm [38]), the identification is not conclusive. Sulfur, sulfate, and other compounds may be present. More careful TEM studies with SAED and EELS could elucidate the oxidation/ degradation kinetics and reaction products of these types of metal chalcogenide films.

IV. CONCLUSIONS

The findings of this work are summarized subsequently.

1. Lattice image and dark-field TEM techniques have been used to investigate the early-growth nanostructure of sputter-deposited MoS_2 solid lubricant films grown under conditions that yield a zone 2 morphology. The near-interface structure consists of anisotropic, platelike islands in which the (001) basal planes are parallel to the plates. The islands have two general orientations: (1) an "edge island" in which the (100) or (110) edge-plane surface is parallel to the substrate or (2) a "basal island" in which the (001) basal plane is parallel to the substrate. Within the context of an active-sites nucleation model, the TEM data show that localized regions of the substrate in an early-growth zone 2 morphology can lack the active sites needed to induce edge orientation, a fact that modifies the original model. The edge islands evolve into the zone 2 morphology, shadowing and inhibiting the continued growth of the basal islands.

2. Films deposited at AT and at HT (220°C) have essentially the same plate dimensions near the interface region, while previous SEM studies have shown that the HT plates become larger than AT plates in thicker films. These TEM results suggest that the substrate surface strongly influences adatom mobility during the early phase of film deposition. Chemical modification of the substrate surface could affect film nucleation.

3. SAED indicates that relative to a MoS_2 standard, the (001) basal planes in the sputter-deposited films are dilated and the (100) and (110) edge planes are contracted. These results agree with earlier XRD studies of thicker films. The distortion in the sputter-deposited films is believed to be caused by the substitution of oxygen for sulfur.

4. Basal plane (002) lattice image curvature and kinking were observed in the edge islands. Dark-field analysis revealed intensity variations within the edge islands. The edge island plates appear to be imperfect crystals of aligned basal planes. These crystals can bend, kink, or twist, apparently as a result of variations in local growth conditions. Image simulation is needed to confirm this interpretation. This ability of crystal growth to deviate has implications for the morphological evolution of thicker films. The ability of MoS_2 to bend supports the idea that localized deformation can occur during sliding or rolling contact.

5. Film morphology changed over a period of months, apparently as a result of film oxidation. Further study is needed to determine reaction products and kinetics.

REFERENCES

1. M. N. Gardos, "Quality Control of Sputtered MoS_2 Films," <u>Lubr. Eng.</u> <u>32</u>, 463 (1976).

2. R. I. Cristy, "Sputtered MoS_2 Lubricant Improvements," <u>Thin Solid Films</u> <u>73</u>, 299 (1980).

3. B. C. Stupp, "Synergistic Effects of Metals Co-Sputtered with MoS_2," <u>Thin Solid Films</u> <u>84</u>, 257 (1981).

4. P. Niederhauser, H. E. Hintermann, and M. Maillat, "Moisture-Resistant MoS_2-Based Composite Lubricant Films," <u>Thin Solid Films</u> <u>108</u>, 209 (1983).

5. B. C. Stupp, "Performance of Conventionally Sputtered MoS_2 Versus Co-Sputtered MoS_2 and Nickel," <u>Proc. 3rd Int. Conf. on Solid Lubrication, Denver, Colo.</u>, American Society of Lubrication Engineers, Park Ridge, Ill., SP-14 (1984), p. 217.

6. T. Spalvins, "Lubrication with Sputtered MoS_2 Films," <u>ASLE Trans.</u> <u>14</u>, 267 (1971).

7. T. Spalvins, "Structure of Sputtered Molybdenum Disulfide Films at Various Substrate Temperatures," <u>ASLE Trans.</u> <u>17</u>, 1 (1973).

8. M. Nishimura, M. Nosaka, M. Suzuki, and Y. Miyakawa, "The Friction and Wear of Sputtered Molybdenum Disulphide Films in Sliding Contact," <u>Proc. 2nd ASLE Int. Sol. Lubr. Conf., 1978, Denver, Colo.</u>, ASLE SP-6, p. 128.

9. T. Spalvins, "Tribological Properties of Sputtered MoS_2 Films in Relation to Film Morphology," <u>Thin Solid Films</u> <u>73</u>, 291 (1980).

10. T. Spalvins, "Morphological and Frictional Behavior of Sputtered MoS_2 Films," <u>Thin Solid Films</u> <u>96</u>, 17 (1982).

11. V. Buck, "Morphological Properties of Sputtered MoS_2 Films," <u>Wear</u> <u>91</u>, 281 (1983).

12. P. D. Fleischauer, "Effect of Crystallite Orientation on the Environmental Stability and Lubrication Properties of Sputtered MoS_2 Thin Films," <u>ASLE Trans.</u> <u>27</u>, 82 (1984).

13. T. Spalvins, "Characteristic Morphological and Frictional Changes in Sputtered MoS_2 Films," <u>Proc. 3rd Int. Conf. on Solid Lubrication, Denver, Colo.</u>, American Society of Lubrication Engineers, Park Ridge, Ill., SP-14, p. 401.

14. R. Bichsel, P. Buffat, and F. Levy, "Correlation Between Process Conditions, Chemical Composition and Morphology of MoS_2 Films Prepared by RF Planar Magnetron Sputtering," J. Phys. D: Appl. Phys. 19, 1575 (1986).

15. V. Buck, "A Neglected Parameter (Water Contamination) in Sputtering MoS_2 Films," Thin Solid Films 139, 157 (1986).

16. V. Buck, "Structure and Density of Sputtered MoS_2 Films," Vacuum 36, 89 (1986).

17. E. W. Roberts, "Towards an Optimized Sputtered MoS_2 Lubricant Film," 20th American Mechanisms Symp., NASA Lewis Res. Ctr., Cleveland, OH. (May 1986), p. 103.

18. E. W. Roberts, "The Tribology of Sputtered Molybdenum Disulphide Films," Proc. Inst. Mech. Eng., Tribology -- Friction, Lubrication, and Wear, Fifty Years On, Vol. I (London, July 1987), p. 503.

19. J. K. G. Panitz, L. E. Pope, C. R. Hills, J. E. Lyons, and D. J. Staley, "A Statistical Study of the Combined Effects of Substrate Temperature, Bias, Annealing and a Cr_3Si_2 Undercoating on the Tribological Properties of R.F. Sputtered MoS_2 Coatings," Thin Solid Films 154, 323 (1987).

20. J. R. Lince and P. D. Fleischauer, "Crystallinity of RF-Sputtered MoS_2 Films," J. Mater. Res. 2(6), 827 (1987).

21. N. J. Mikkelson, J. Chevallier, and G. Sorenson, "Friction and Wear Measurements of Sputtered MoS_x Films Amorphized by Ion Bombardment," Appl. Phys. Lett. 52, 1130 (1988).

22. P. D. Fleischauer and R. Bauer, "Chemical and Structural Effects on the Lubrication Properties of Sputtered MoS_2 Films," Tribology Transactions 31, 239 (1988).

23. C. Müller, C. Menoud, M. Maillat, and H. E. Hintermann, "Thick Compact MoS_2 Coatings," Surface Coatings and Technol. 36, 351 (1988).

24. M. R. Hilton and P. D. Fleischauer, Mat. Res. Soc. Symp. Proc. 140 227, (1989).

25. P. Gribi, Z. W. Sun, and F. Levy, "Effects of Low-Energy Ion Bombardment on RF Sputtered MoS_{2-x} Films," J. Appl. Phys. D: Appl. Phys. 22, L238 (1989).

26. a. J. A. Thornton, "High Rate Thick Film Growth," Ann. Rev. Mater. Sci. 7, 239 (1977).

   b. J. A. Thornton, "The Microstructure of Sputter-Deposited Coatings," J. Vac. Sci. & Technol. A 4(6), 3059 (1986).

27. B. A. Movchan and A. V. Demchishin, "Investigation of the Structure and Properties of Thick Vacuum-Deposited Films of Nickel, Titanium, Tungsten, Aluminum, and Zirconium Dioxide," Phy. Met. Metallogr. 28, 83 (1969).

28. P. A. Bertrand, "Orientation of RF-Sputter-Deposited MoS_2 Films," J. Mater. Res. 4(1), 180 (1989).

29. S. V. Didziulis and P. D. Fleischauer, "The Effects of Chemical Treatments on SiC Surface Composition and Subsequent MoS_2 Film Growth," Langmuir 6, 621 (1990).

30. M. Matsunaga and T. Nakagawa, "Frictional Behavior of Various Kinds of Molybdenum Disulfide," Proc. 2nd. Int. Conf. on Solid Lubrication, 1978, Denver, Colo., ASLE SP-6, p. 45.

31. M. T. Lavik and M. E. Campbell, "Evidence of Crystal Structure in Some Sputtered MoS_2 Films," ASLE Transactions (1971-1972), p. 233.

32. G. G. Shaw and M. T. Lavik, "Technique for Examining the Structure of Sputtered MoS_2 Lubrication Films by Ion Erosion and Transmission Electron Microscopy," Proc. Electron Micros. Soc. Amer. 30, 626 (1972).

33. P. A. Bertrand, "Interfacial Chemistry of MoS_2 Films on Si," Langmuir 5, 1387 (1989).

34. J. R. Lince, "$MoS_{2-x}O_x$ Solid Solutions in Thin Films Produced by RF-Sputter Deposition," J. Mater. Res. 5(1), 218 (1990).

35. P. D. Fleischauer, "Fundamental Aspects of the Electronic Structure, Materials Properties and Lubrication Performance of Sputtered MoS_2 Films," Thin Solid Films 154, 309 (1987).

36. P. D. Fleischauer, J. R. Lince, P. A. Bertrand, and R. Bauer, "Electronic Structure and Lubrication Properties of MoS_2: A Qualitative Molecular Orbit Approach," Langmuir 5, 1009 (1989).

37. Powder Diffraction File (JCPDS International Center for Diffraction Data, Swarthmore, Pa., 1983).

38. B. D. Cullity, Elements of X-Ray Diffraction (Addison-Wesley, 1978), p. 284.

47

39. G. Thomas and M. J. Goringe, Transmission Electron Microscopy of Materials (Wiley-Interscience, 1979), p. 191.

40. J. W. Edington, Practical Electron Microscopy in Materials Science, Monograph 3: Interpretation of Transmission Electron Micrographs (MacMillan Technical Library, 1975), p. 75.

41. J. C. H. Spence, Experimental High-Resolution Electron Microscopy (Clarendon Press, Oxford, 1981).

42. K. C. Thompson-Russell and J. W. Edington, Practical Electron Microscopy in Materials Science, Monograph 5: Electron Microscope Specimen Preparation Techniques in Materials Science (MacMillan Technical Library, 1977), p. 21.

43. D. R. Veblen and P. R. Buseck, "Serpentine Materials: Intergrowths and New Combination Structures," Science 206, 1398 (1979).

44. J. V. Sanders, "High Resolution Microscopy of Some Catalytic Particles," Chemica Scripta 79, (14), 141 (1978).

45. O. Sorensen, B. S. Clausen, R. Candia, and H. Topsoe, "HREM and AEM Studies of HDS Catalysts: Direct Evidence for the Edge Location of Cobalt in Co-Mo-S," Applied Catalysis 16, 363 (1985).

46. F. Delannay, "High Resolution Electron Microscopy of Hydrodesulfurization Catalysts: A Review," Applied Catalysis 16, 135 (1985).

47. N. Takahashi, "Direct Resolution of the Layer Lattice of Molybdenum Disulfide by Transmission Electron Microscopy in Relation to Lubrication," Wear 124, 279-289 (1988).

48. J. R. Jones and G. W. Hoover, "Abrasiveness of MoS_2 in Bonded Solid Lubricants," ASLE Trans. 14, 55 (1971).

49. M. N. Gardos, "The Synergistic Effect of Graphite on the Friction and Wear of MoS_2 Films in Air," Tribology Trans. 31(2), 214 (1988).

50. JANAF Thermochemical Tables, 2nd ed., National Bureau of Standards, Washington, D.C. (June 1971).

LABORATORY OPERATIONS

The Aerospace Corporation functions as an "architect-engineer" for national security projects, specializing in advanced military space systems. Providing research support, the corporation's Laboratory Operations conducts experimental and theoretical investigations that focus on the application of scientific and technical advances to such systems. Vital to the success of these investigations is the technical staff's wide-ranging expertise and its ability to stay current with new developments. This expertise is enhanced by a research program aimed at dealing with the many problems associated with rapidly evolving space systems. Contributing their capabilities to the research effort are these individual laboratories:

Aerophysics Laboratory: Launch vehicle and reentry fluid mechanics, heat transfer and flight dynamics; chemical and electric propulsion, propellant chemistry, chemical dynamics, environmental chemistry, trace detection; spacecraft structural mechanics, contamination, thermal and structural control; high temperature thermomechanics, gas kinetics and radiation; cw and pulsed chemical and excimer laser development, including chemical kinetics, spectroscopy, optical resonators, beam control, atmospheric propagation, laser effects and countermeasures.

Chemistry and Physics Laboratory: Atmospheric chemical reactions, atmospheric optics, light scattering, state-specific chemical reactions and radiative signatures of missile plumes, sensor out-of-field-of-view rejection, applied laser spectroscopy, laser chemistry, laser optoelectronics, solar cell physics, battery electrochemistry, space vacuum and radiation effects on materials, lubrication and surface phenomena, thermionic emission, photosensitive materials and detectors, atomic frequency standards, and environmental chemistry.

Electronics Research Laboratory: Microelectronics, solid-state device physics, compound semiconductors, radiation hardening; electro-optics, quantum electronics, solid-state lasers, optical propagation and communications; microwave semiconductor devices, microwave/millimeter wave measurements, diagnostics and radiometry, microwave/millimeter wave thermionic devices; atomic time and frequency standards; antennas, rf systems, electromagnetic propagation phenomena, space communication systems.

Materials Sciences Laboratory: Development of new materials: metals, alloys, ceramics, polymers and their composites, and new forms of carbon; nondestructive evaluation, component failure analysis and reliability; fracture mechanics and stress corrosion; analysis and evaluation of materials at cryogenic and elevated temperatures as well as in space and enemy-induced environments.

Space Sciences Laboratory: Magnetospheric, auroral and cosmic ray physics, wave-particle interactions, magnetospheric plasma waves; atmospheric and ionospheric physics, density and composition of the upper atmosphere, remote sensing using atmospheric radiation; solar physics, infrared astronomy, infrared signature analysis; effects of solar activity, magnetic storms and nuclear explosions on the earth's atmosphere, ionosphere and magnetosphere; effects of electromagnetic and particulate radiations on space systems; space instrumentation.